A COMPARATIVE ASSESSMENT AMONG ITERATIVE LINEAR SOLVERS DEALING WITH ELECTROMAGNETIC INTEGRAL EQUATIONS IN 3D INHOMOGENEOUS ANISOTROPIC MEDIA

G. Franceschini, A. Abubakar, T. M. Habashy, and A. Massa

A Comparative Assessment among Iterative Linear Solvers dealing with Electromagnetic Integral Equations in 3D Inhomogeneous Anisotropic Media

G. Franceschini[(1)], A. Abubakar[(2)], T. M. Habashy[(2)], and A. Massa[(1)]

[(1)] Department of Information and Communication Technologies

University of Trento, Via Sommarive 14, 38050 Trento - Italy

Tel. +39 0461 882057, Fax +39 0461 882093

E-mail: *andrea.massa@ing.unitn.it*, {*gabriele.franceschini*} *@dit.unitn.it*

Web: *http://www.eledia.ing.unitn.it*

[(2)] Schlumberger-Doll Research

36 Old Quarry Road, Ridgefield, CT-06877 - USA

Tel. +1 203 431 5000, Fax +1 203 438 3819

E-mail: {*aabubakar*, *thabashy*} *@ridgefield.oilfield.slb.com*,

A Comparative Assessment among Iterative Linear Solvers dealing with Electromagnetic Integral Equations in 3D Inhomogeneous Anisotropic Media

Gabriele Franceschini, Aria Abubakar, Tarek M. Habashy, and Andrea Massa

Abstract

This paper deals with full-vectorial, three-dimensional, electromagnetic scattering problems formulated in terms of integral scattering equations. The weak formulation is applied in order to effectively deal with inhomogeneous anisotropic media and the arising set of algebraic linear equations is solved through some of the most recent and effective iterative linear solvers for allowing a detailed assessment of their performances when facing with three-dimensional complex scenarios.

Index Terms - Electromagnetic Scattering, Forward Problem, Three-Dimensional Geometry, Anisotropic Media, Integral Equations, Weak-Formulation.

1 Introduction

Modeling electromagnetic fields in realistic three-dimensional (*3D*) scenarios is an appealing research topic. However, the solution of the arising electromagnetic scattering problems is a critical issue since it requires the use of numerical procedures with a non-negligible computational load, especially when large and complex realistic configurations are taken into account.

As far as two-dimensional (*2D*) geometries and dissipative objects are concerned, *Richmond* proposed in [1] the use of the Method of Moments (*MoM*). A stiffness matrix, whose dimensions depend on the size of the investigation domain, the working frequency, and the contrast of the dielectric objects, is generated and successively inverted. The need of inverting such a matrix strongly limits the application of the *MoM* especially when the problem size grows. In order to reduce the computational load and the required large amount of computer memory, the so-called *k-Space Method* has been introduced [2]. Such an approach combines an iterative approach and the Fast Fourier Transform (*FFT*) algorithm for efficiently computing the spatial convolution operator that occurs in the integral scattering equations [3]. A further improvement, concerned with 2D-TM configurations, has been successfully obtained by applying the Conjugate Gradient Fast Fourier Transform (*CG-FFT*) [4][5][6][7][8][9].

Concerning 2D-TE scenarios, the problem has been addressed by *Zwamborn and van den Berg* [10] developing a weak-form of the integral scattering. A successive extension to 3D isotropic cases has been presented in [11] and further improved for allowing a more easy and effective numerical implementation [12][13].

In this paper, the approach presented in [13] is reformulated for dealing with 3D inhomogeneous anisotropic media. The solution of the arising algebraic linear system is addressed by means of a set of iterative solvers and the performances of the Conjugate Gradient (*CG*) approach, the BiConjugate Gradient (*BiCG*) method, the Stabilized BiConjugate Gradient (*BiCGStab*) technique, the Quasi Minimal Residual (*QMR*) method, and the Generalized Minimal Residual (*GMRES*) algorithm are then compared. To the best of authors' knowledge, although detailed analyzes have been carried out on weak-form-based techniques ([10][11][12][13][14][15]), this is the first time that an exhaustive comparison on

iterative solvers when dealing with inhomogeneous anisotropic 3D geometries is carried out.

The paper is organized as follows. In Section 2, the integral formulation of the three-dimensional anisotropic problem is presented. The results of a comparative study among effective iterative linear solvers are shown in Section 3. Some conclusions are eventually presented in Section 4.

2 Mathematical Formulation

Let us consider a data domain R and a computational (or investigation) domain D generally composed by an inhomogeneous anisotropic medium of finite dimension and embedded in a homogeneous isotropic background of constant permittivity ε_b, electric conductivity σ'_b, and permeability μ_b. Such a scenario is illuminated by a known electromagnetic source defined on a support S and described through the impressed electric, $\overline{\mathbf{J}}\left(\overline{\mathbf{r}}^S\right)$, $\overline{\mathbf{r}}^S \in S$, and magnetic, $\overline{\mathbf{K}}\left(\overline{\mathbf{r}}^S\right)$, current densities.

By considering a Cartesian coordinate system, a time-harmonic temporal dependence, and non-magnetic materials, the electric field satisfies the following equation

$$
\begin{aligned}
\overline{\bigtriangledown} \times \overline{\bigtriangledown} \times \overline{\mathbf{E}}\left(\overline{\mathbf{r}}\right) - k_b^2 \overline{\mathbf{E}}\left(\overline{\mathbf{r}}\right) = \\
k_b^2 \overline{\overline{\mathbf{Q}}}\left(\overline{\mathbf{r}}\right) \cdot \overline{\mathbf{E}}\left(\overline{\mathbf{r}}\right) + \mathrm{i}\omega\mu_b \overline{\mathbf{J}}\left(\overline{\mathbf{r}}^S\right) - \overline{\bigtriangledown} \times \overline{\mathbf{K}}\left(\overline{\mathbf{r}}^S\right),
\end{aligned}
\tag{1}
$$

where $k_b^2 = \mathrm{i}\omega\mu_b\sigma_b$, $\sigma_b = \sigma'_b - \mathrm{i}\omega\varepsilon_b$, and $\overline{\overline{\mathbf{Q}}}\left(\overline{\mathbf{r}}\right)$ is the contrast function describing the anisotropic investigation domain

$$
\overline{\overline{\mathbf{Q}}}\left(\overline{\mathbf{r}}\right) = \frac{1}{\sigma_b}\begin{bmatrix} \sigma_{xx}\left(\overline{\mathbf{r}}\right) - \sigma_b & \sigma_{xy}\left(\overline{\mathbf{r}}\right) & \sigma_{xz}\left(\overline{\mathbf{r}}\right) \\ \sigma_{xy}\left(\overline{\mathbf{r}}\right) & \sigma_{yy}\left(\overline{\mathbf{r}}\right) - \sigma_b & \sigma_{yz}\left(\overline{\mathbf{r}}\right) \\ \sigma_{xz}\left(\overline{\mathbf{r}}\right) & \sigma_{yz}\left(\overline{\mathbf{r}}\right) & \sigma_{zz}\left(\overline{\mathbf{r}}\right) - \sigma_b \end{bmatrix}, \quad \overline{\mathbf{r}} \in D \tag{2}
$$

By applying the Green's theorem and the radiation condition at infinity, the problem mathematically described through Eq. (1) is reformulated in integral form by writing the

4

following relationship

$$\overline{\mathbf{E}}_b(\overline{\mathbf{r}}) = \Omega\left[\overline{\mathbf{E}}(\overline{\mathbf{r}})\right] = \overline{\mathbf{E}}(\overline{\mathbf{r}}) - \left[k_b^2\,\overline{\overline{\mathbf{I}}} + \overline{\nabla}\,\overline{\nabla}\right]\cdot\overline{\mathbf{A}}(\overline{\mathbf{r}}), \tag{3}$$

where $\overline{\mathbf{E}}_b(\overline{\mathbf{r}})$ is the electric field in a homogeneous and unbounded background of complex conductivity σ_b and permeability μ_b, $\overline{\overline{\mathbf{I}}}$ is the unit dyadic and

$$\overline{\mathbf{A}}(\overline{\mathbf{r}}) = \int_D g(\overline{\mathbf{r}},\overline{\mathbf{r}}')\,\overline{\overline{\mathbf{Q}}}(\overline{\mathbf{r}}')\cdot\overline{\mathbf{E}}(\overline{\mathbf{r}}')\,\mathrm{d}\overline{\mathbf{r}}' \tag{4}$$

is the electric vector potential, the scalar Green function $g(\overline{\mathbf{r}},\overline{\mathbf{r}}')$ being

$$g(\overline{\mathbf{r}},\overline{\mathbf{r}}') = \frac{\exp(\mathrm{i}k_b|\overline{\mathbf{r}} - \overline{\mathbf{r}}'|)}{4\pi|\overline{\mathbf{r}} - \overline{\mathbf{r}}'|}. \tag{5}$$

In order to numerically compute $\overline{\mathbf{E}}(\overline{\mathbf{r}})$, the domain D is partitioned using a uniform grid of rectangular cells of side $\Delta x \times \Delta y \times \Delta z$ where the contrast $\overline{\overline{\mathbf{Q}}}$ is assumed to be constant. According to the procedure described in [13], the integral operators are discretized by applying the weakening procedure in order to cope with the singularity and the spatial differentiation operators are calculated by using the finite difference rule. In order to properly deal with anisotropic media, the electric vector potential $\overline{\mathbf{A}}(\overline{\mathbf{r}})$ is numerically-evaluated as follows

$$A^{(h)}(\overline{\mathbf{r}}_{m,n,p}) = \Delta x \Delta y \Delta z \sum_{m'=1}^{M}\sum_{n'=1}^{N}\sum_{p'=1}^{P} g\left(\overline{\mathbf{r}}_{m,n,p},\,\overline{\mathbf{r}}_{m',n',p'}\right)$$
$$\sum_{k=x,y,z} Q^{(h,k)}\left(\overline{\mathbf{r}}_{m',n',p'}\right) E^{(k)}\left(\overline{\mathbf{r}}_{m',n',p'}\right) \tag{6}$$
$$h, k = x, y, z;\; m = 1,...,M;\; n = 1,...,N;\; p = 1,...,P;$$

where $\overline{\mathbf{r}}_{m,n,p}$ identifies the generic center-point of a volumetric sub-domain belonging to the investigation area; M, N and P are the numbers of discretizations along $\hat{\mathbf{x}}$, $\hat{\mathbf{y}}$ and $\hat{\mathbf{z}}$, respectively; $E^{(k)}$ denotes the k-th component of $\overline{\mathbf{E}}$, and $g(\overline{\mathbf{r}}_{m,n,p}, \overline{\mathbf{r}}_{m',n',p'})$ is computed as in [13]. By applying the convolution theorem of Discrete Fourier Transform (DFT), it turns out that

5

$$A^{(h)}\left(\overline{\mathbf{r}}_{m,n,p}\right) = \Delta x \Delta y \Delta z DFT^{-1}\left\{DFT\left[g\left(\overline{\mathbf{r}}_{m,n,p}\right)\right]B^{(h)}\left(\overline{\mathbf{r}}_{m,n,p}\right)\right\}$$
$$h = x, y, z; \; m = 1, ..., M; \; n = 1, ..., N; \; p = 1, ..., P; \tag{7}$$

where

$$B^{(h)}\left(\overline{\mathbf{r}}_{m,n,p}\right) = DFT\left[\sum_{k=x,y,z}Q^{(h,k)}\left(\overline{\mathbf{r}}_{m,n,p}\right)E^{(k)}\left(\overline{\mathbf{r}}_{m,n,p}\right)\right],$$
$$h = x, y, z; \; m = 1, ..., M; \; n = 1, ..., N; \; p = 1, ..., P. \tag{8}$$

thus allowing a computationally-efficient computation through FFT routines.

After discretization, the prediction problem is then recasts as the solution of the arising linear system of $U = 3 \times M \times N \times P$ equations where the electric field of the background, $E_{b,syn}^{(k)}\left(\overline{\mathbf{r}}_{m,n,p}\right)$, $k = x, y, z$, $m = 1, ..., M$, $n = 1, ..., N$, $p = 1, ..., P$, is a known quantity because of the knowledge of the electromagnetic source. Towards this end, because of the well-posed nature of the forward problem at hand [17], effective linear iterative solvers [namely, the well-known Conjugate Gradient (CG) approach, the Bi-Conjugate Gradient ($BiCG$) method [14][18] and its stabilized version ($BiCGStab$) [15], the Quasi-Minimal Residual (QMR) approach [19], and the Generalized Minimum Residual ($GMRES$) method or its restarted implementation [20] ($R - GMRES$)] aimed at minimizing the distance ρ_i (i being the iteration index) between the estimated solution and the actual one, can be profitably used thus avoiding time-consuming inversion procedures. More in detail, let us define the "*residual*" vector $\overline{\mathbf{u}}_i$, an array of dimension U whose components are given by

$$u_{m,n,p}^{i(k)} = E_b^{i(k)}\left(\overline{\mathbf{r}}_{m,n,p}\right) - E_{b,syn}^{(k)}\left(\overline{\mathbf{r}}_{m,n,p}\right) \qquad \begin{matrix} k = x, y, z; \; m = 1, ..., M; \\ n = 1, ..., N; \; p = 1, ..., P, \end{matrix} \tag{9}$$

$E_b^{i(k)}\left(\overline{\mathbf{r}}_{m,n,p}\right)$ being computed through (3) on the basis of the trial solution estimated at the i-th iteration, $E_i^{(k)}\left(\overline{\mathbf{r}}_{m,n,p}\right)$, of the iterative process. Then, the distance is computed as

$$\rho_i = \frac{\sqrt{\sum_{k=x,y,z} \sum_{m=1}^{M} \sum_{n=1}^{N} \sum_{p=1}^{P} \left| u_{m,n,p}^{i(k)} \right|^2}}{\sqrt{\sum_{k=x,y,z} \sum_{m=1}^{M} \sum_{n=1}^{N} \sum_{p=1}^{P} \left| E_{b,syn}^{(k)} \left(\overline{\mathbf{r}}_{m,n,p} \right) \right|^2}}. \tag{10}$$

and minimized by generating a convergent sequence of trial solutions $\left\{ E_i^{(k)} \left(\overline{\mathbf{r}}_{m,n,p} \right) ; \, i = 1, ..., I \right\}$ according to a suitable iterative approach.

Finally, once the distribution of $E^{(k)} \left(\overline{\mathbf{r}}_{m,n,p} \right)$, $k = x, y, z$; $m = 1, ..., M$; $n = 1, ..., N$; $p = 1, ..., P$; $\forall k = x, y, z$, $m = 1, ..., M$, $n = 1, ..., N$, $p = 1, ..., P$ is determined, also the scattered magnetic field at $\overline{\mathbf{r}}^R \in R$ can be easily computed through the following relationship

$$\overline{\mathbf{H}}^{scatt} \left(\overline{\mathbf{r}}^R \right) = \sigma_b \overline{\nabla}^R \times \overline{\mathbf{A}} \left(\overline{\mathbf{r}}^R \right). \tag{11}$$

3   Numerical Validation

In this section, the performances of the set of representative linear iterative solvers are compared by considering, as a reference benchmark, the electromagnetic problem modeling the system for the electromagnetic induction well logging largely used in the oil exploration.

As far as the electromagnetic source is concerned, it is a point magnetic dipole directed along the $\overline{\nu}$-direction and represented through a null electric density $(\overline{\mathbf{J}} = 0)$ and an impulsive magnetic current $(\overline{\mathbf{K}} \left(\overline{\mathbf{r}}^S \right) = \delta \left(\overline{\mathbf{r}}^S \right) \overline{\nu}$. Consequently, the electric field in the background is given by

$$\overline{\mathbf{E}}_{b,syn} \left(\overline{\mathbf{r}}_{m,n,p} \right) = -\overline{\nabla} \times g \left(\overline{\mathbf{r}}_{m,n,p}, \overline{\mathbf{r}}^S \right) \overline{\nu} = -\overline{\mathbf{h}} \left(\overline{\mathbf{r}}_{m,n,p}, \overline{\mathbf{r}}^S \right) \times \overline{\nu}$$
$$m = 1, ..., M; \, n = 1, ..., N; \, p = 1, ..., P \, ; \tag{12}$$

where

$$h^{(k)}\left(\overline{\mathbf{r}}_{m,n,p}, \ \overline{\mathbf{r}}^S\right) = -\frac{g\left(\overline{\mathbf{r}}_{m,n,p}, \overline{\mathbf{r}}^S\right)}{\left|\overline{\mathbf{r}}_{m,n,p} - \overline{\mathbf{r}}^S\right|} \frac{r^{(k)} - r^{S(k)}}{\left|\overline{\mathbf{r}}_{m,n,p} - \overline{\mathbf{r}}^S\right|} \left[1 - \mathrm{i}k_b \left|\overline{\mathbf{r}}_{m,n,p} - \overline{\mathbf{r}}^S\right|\right] \tag{13}$$

$$k = x, y, z; \ m = 1, ..., M; \ n = 1, ..., N; \ p = 1, ..., P \ .$$

In the first test case, the probing system consists of: (a) an electromagnetic source working at frequency $f_0 = 1 \ KHz$ and located at $\overline{\mathbf{r}}^S = (-50, 0, 0) \, m \ [\overline{\mathbf{r}}^S \in D]$, (b) $N^R = 41$ receivers located at $\overline{\mathbf{r}}_j^R = \left[50, 0.0, 5.0 \times \left(j - \frac{N^R - 1}{2}\right)\right] m, \ j = 0, ..., (N^R - 1)$. Concerning the cubical computational domain D, it is inhomogeneous, $l_D = 50 \, m$ in side, and it has been partitioned into a grid of $32 \times 32 \times 32$ cells. Two homogeneous isotropic cubic objects $l_{obj} = 12.5 \, m$-sided and characterized by a conductivity $\sigma_{xx}^{(1)} = \sigma_{yy}^{(1)} = \sigma_{zz}^{(1)} = 10 \, \frac{S}{m}$ and $\sigma_{xx}^{(2)} = \sigma_{yy}^{(2)} = \sigma_{zz}^{(2)} = 10^{-2} \, \frac{S}{m}$ lie in D at the locations $C_1 = (-12.5, -12.5, -12.5) \, m$ and $C_2 = (12.5, 12.5, 12.5) \, m$, respectively. The isotropic background is homogeneous with a constant conductivity equal to $\sigma_b = 0.1 \, \frac{S}{m}$.

As far as the iterative process is concerned, the minimization has been stopped when the condition $(\rho_i < 10^{-7})$ was satisfied and the prediction results are shown in Fig. 1 in terms of the values of the magnetic field components at the measurement points in R. As it can be observed, the plots related to each solver are almost indistinguishable, but significant differences turns out in terms of the computational load and convergence.

Figure 2 shows the behavior of the error function ρ_i versus the iteration number j pointing out its monotonic decreasing when the CG, $GMRES$ and $R - GMRES$ techniques are used. On the other hand, the remaining approaches (and in particular the $BiCG$ technique) seem to be unstable with fast variations in the values of ρ_i. However, its should noticed that the convergence ratio of the $BiCG$ method significantly improves compared to the standard CG reducing ten times the number of iterations for reaching the convergence threshold [see Table I where the average CPU-time per iteration $(\overline{t_i})$ together with the convergence index (I_{conv}), the initialization time (t_0), and the total CPU-time (T) are given]. Moreover, with reference to Figure 3 and Table I, it turns out that the CG, the $BiCG$, and the QMR need of the same amount of CPU-time per iteration $\overline{t_i}$ since their computational costs are due to the evaluations (i.e., two evaluations at each iteration) of the operator Ω and the remaining vector/scalar product operations

require a negligible amount of CPU-time (if compared to the Ω evaluation).

A significant improvement of the computational performances is obtained by using the $BiCGStab$ technique since, in addition to a slight reduction of the time per iteration t_i due to the smaller number of vectorial products at each iteration, the total number of iterations is almost halved when compared to those of the $BiCG$ approach. A further improvement is achieved by the $GMRES$ technique since it requires only one computation of the operator Ω per iteration even though the CPU-time grows linearly with the number of iterations because of the increasing of the dimension of the Hessenberg matrix. Such a behavior results in the quadratic dependence of the computation time T_i as shown in Fig. 4.

In order to avoid the drawback related to the matrix storage of the $GMRES$, the $R-GMRES$ method has been evaluated, as well, by setting $I_{res} = 20$. Although, on average, t_i decreases, such an approach presents a slower convergence ratio (Fig. 2) than the $GMRES$ and furthermore, an extra time is needed at each restart as shown in Figure 3. Such an event further confirms the reliability and the computational effectiveness of the $GMRES$.

In the second test case, the water-oil contact model shown in Figure 5 is considered. In such a case, the computational domain of size $6.4 \times 6.4 \times 12.8 \, m^3$ and discretized into $32 \times 32 \times 64$ cells consists of an isotropic deviated water layer with conductivity $\sigma_{xx}^{water} = \sigma_{yy}^{water} = \sigma_{zz}^{water} = 5 \, \frac{S}{m}$ (white color in Fig. 5) and an anisotropic water-oil contact region (black color in Fig. 5) $[\sigma_{xx}^{oil} = \sigma_{yy}^{oil} = 0.333 \, \frac{S}{m}, \, \sigma_{zz}^{oil} = 0.05 \, \frac{S}{m}]$ in a rock background (brown color in Fig. 5) of conductivity $\sigma_r = 1.0 \, \frac{S}{m}$. Both transmitter and receivers have the same locations of the previous example, but the operating frequency is equal to $f_0 = 26.3 \, KHz$.

Figure 6 shows the behavior of the predicted magnetic field at the locations of the receivers. As expected, whatever the approach, the field behavior is faithfully estimated. Consequently, the computational effectiveness turns out to be the index of success among the different solution techniques.

From the computational point-of-view and with reference to Figures 7-9 and Table II, similar conclusions to those concerned with the first test case hold true. However, despite

the greater number of discretization cells and the configuration complexity, the convergence ratio is on average faster than that of the previous test case (see Fig 7), but the CPU-time per iteration increases (Tab. II). Thanks to the non-negligible reduction of the required iterations (I_{conv}) in comparison with those of the other techniques, the total amount of CPU-time required by the $BiCGStab$ is comparable with that needed for the $GMRES$ method.

As far as the $R-GMRES$ solver is concerned, I_{res} has been fixed to $I_{res}=5$. This is a smaller value than that in the first example, since the amount of memory used per iteration significantly grows. Consequently, the initialization time at each restart has a significant influence on the total CPU-time and therefore, the $R-GMRES$ method is slower than its standard implementation.

Finally, it should be observed that in such an example the ratio between the computational costs of the fastest and the slowest algorithm significantly enlarges ($\frac{T_{CG}}{T_{GMRES}} \simeq 19$ - Test Case 2 vs. $\frac{T_{CG}}{T_{GMRES}} \simeq 8.3$ - Test Case 1) because of the slower convergence of the CG method ($I_{conv}^{CG} = 1556$ - Test Case 1 vs. $I_{conv}^{CG} = 110$ - Test Case 2).

4 Conclusions

In this paper, a comparative assessment among iterative linear solvers when dealing with three-dimensional inhomogeneous and anisotropic media has been carried out. As expected, the numerical results confirmed the effectiveness of the considered approaches concerning the accuracyin the electromagnetic prediction. On the other hand, the numerical study showed that the $GMRES$ method is the fastest solver even though the corresponding CPU-time per iteration linearly increases. Moreover, the required amount of memory depends on the number of iterations for reaching convergence in a proportional way. Consequently, the $GMRES$ turns out to be a suitable technique only when a large amount of memory is available or when small-scale problems are dealt with. On the contrary, the obtained results pointed out that it is profitable to use the $BiCGStab$ algorithm when the computational domain becomes larger and larger. As a matter of fact, such an approach presented comparable or better performances than the $R-GMRES$, but avoiding those drawbacks concerned with the memory requirements.

References

[1] J. H. Richmond, "Scattering by a dielectric cylinder of arbitrary cross section," *IEEE Trans. Antennas Propagat.*, vol. 13, pp. 334-341, Mar. 1965.

[2] N. N. Bojarski, "K-space formulation of the scattering problem in the time domain," *J. Acoust. Soc. Am.*, vol. 72, pp. 570-584, 1982.

[3] D. Lesselier and B. Duchene, "Buried, 2-D penetrable objects illuminated by line sources: FFT-based iterative computations of the anomalous field," *Progress in Electromagnetics Research, PIER*, vol. 5, pp. 351-389, 1991.

[4] T. K. Sarkar, E. Arvas, and S. M. Rao, "Application of FFT and the conjugate method for the solution of electromagnetic radiation from electrically large and small conducting bodies," *IEEE Trans. Antennas Propagat.*, vol. 34, pp. 635-640, May 1986.

[5] R. Kastner, "A conjugate gradient procedure for analysis of planar conductors with alternating patch and aperture formulation," *IEEE Trans. Antennas Propagat.*, vol. 36, pp. 1616-1620, Nov. 1988.

[6] T. J. Peters and J. L. Volakis, "Application of a conjugate gradient FFT method to scattering from thin planar material plates," *IEEE Trans. Antennas Propagat.*, vol. 36, pp. 518-526, Apr. 1988.

[7] M. F. Catedra, J. G. Cuevas, and L. Nuno, "A scheme to analyze conducting plates of resonant size using the conjugate gradient method and fast Fourier transform," *IEEE Trans. Antennas Propagat.*, vol. 36, pp. 1744-1752, Dec. 1988.

[8] A. F. Peterson, S. L. Ray, C. H. Chen, and R. Mittra, "Numerical implementations of the conjugate gradient method and the CG-FFT for electromagnetic scattering," *Progress in Electromagnetics Research, PIER*, vol. 5, pp. 241-300, 1991.

[9] J. L. Volakis and K. Barkeshli, "Applications of the conjugate gradient FFT method to radiation and scattering," *Progress in Electromagnetics Research, PIER*, vol. 5, pp. 159-239, 1991.

[10] P. Zwamborn and P. M. van den Berg, "A weak form of the conjugate gradient FFT method for two-dimensional TE scattering problems," *IEEE Trans. Microwave Theory Tech.*, vol. 39, pp. 953-960, Jun. 1991.

[11] P. Zwamborn and P. M. van den Berg, "The three-dimensional weak form of the conjugate gradient FFT method for scattering problems," *IEEE Trans. Microwave Theory Tech.*, vol. 40, pp. 1757-1766, Sep. 1992.

[12] A. Abubakar and P. M. van den Berg, Three-dimensional nonlinear inversion in cross-well electrode logging, *Radio Science*, vol. 33, no. 4, pp. 989-1004, 1998.

[13] A. Abubakar and P. M. van den Berg, "Iterative forward and inverse algorithms based on domain integral equations for three-dimensional electric and magnetic objects," *Journal of Computational Physics*, vol. 195, pp. 236-262, 2004.

[14] Z. Q. Zhang and Q. H. Liu, "Three-dimensional weak-form conjugate- and biconjugate-gradient FFT methods for volume integral equations," *Microwave Opt. Technol. Lett.*, vol. 29, pp. 350-356, Jun. 2001.

[15] Z. Q. Zhang and Q. H. Liu, "Applications of the BCGS-FFT method to 3-D induction well logging problems," *IEEE Geosci. Remote Sensing*, vol. 41, pp. 998-1004, May 2003.

[16] J. A. Kong, *Electromagnetic Wave Theory*, New York, USA: John Wiley, 1990.

[17] P. M. van den Berg, "Iterative schemes based on the minimization of the error in field problems," *Electromagnetics*, vol. 5, no. 2-3, pp. 237-262, 1985

[18] H. Gan and W. C. Chew, "A discrete BCG-FFT algorithm for solving 3D inhomogeneous scatterer problems ," *JEMWA*, vol. 9, pp. 1339-1357, 1995.

[19] R. Freund and N. Nachtigal, "QMR: A quasi-minimal residual method for non-hermitian linear systems," *Numer. Math.*, vol. 60, pp. 315-339, 1991.

[20] Y. Saad and M. H. Schultz, "GMRES: a generelized minimal residual algorithm for solving nonsymmetric linear systems," *SIAM J. Sci. Stat. Comput.* , vol. 7, pp. 856-869, Jul. 1986.

Figure Captions

- **Figure 1.** *Test Case I* - Real $(a)(c)(e)$ and imaginary $(b)(d)(f)$ part of the x $(a)(b)$, y $(c)(d)$, and z $(e)(f)$ components of the magnetic field in the data domain S.

- **Figure 2.** *Test Case I* - Normalized error ρ_i versus iteration number i.

- **Figure 3.** *Test Case I* - CPU-time per iteration (t_i).

- **Figure 4.** *Test Case I* - Total CPU-time T_i versus iteration number i.

- **Figure 5.** *Test Case II* - Conductivity distribution of the water-oil contact model. On the left hand side two orthogonal volume slices of the are shown. On the right hand side, 2D conductivity distributions at $y = 0$ and $x = -0.1\,m$. Multi-component data are collected along the vertical axis (i.e., z-axis) that coincides with the wellbore axis.

- **Figure 6.** *Test Case II* - Real $(a)(c)(e)$ and imaginary $(b)(d)(f)$ part of the x $(a)(b)$, y $(c)(d)$, and z $(e)(f)$ components of the magnetic field in the data domain S.

- **Figure 7.** *Test Case II* - Normalized error ρ_i versus iteration number i.

- **Figure 8.** *Test Case II* - CPU-time per iteration (t_i).

- **Figure 9.** *Test Case II* - Total CPU-time T_i versus iteration number i.

Table Captions

- **Table I.** *Test Case I* - Computational indexes.

- **Table II.** *Test Case II* - Computational indexes.
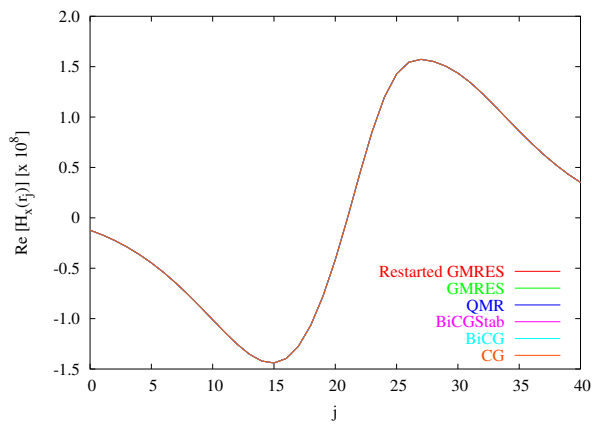
(a)
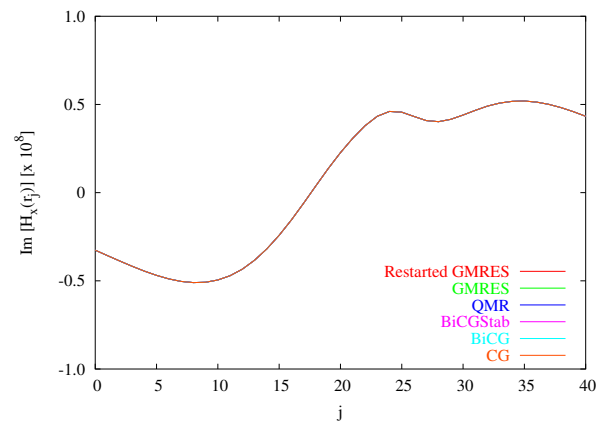
(b)
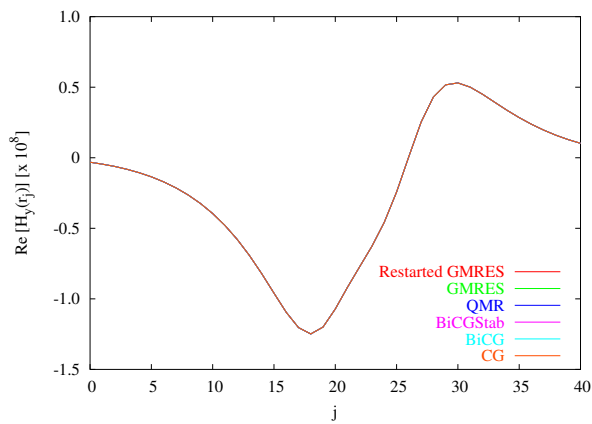
(c)
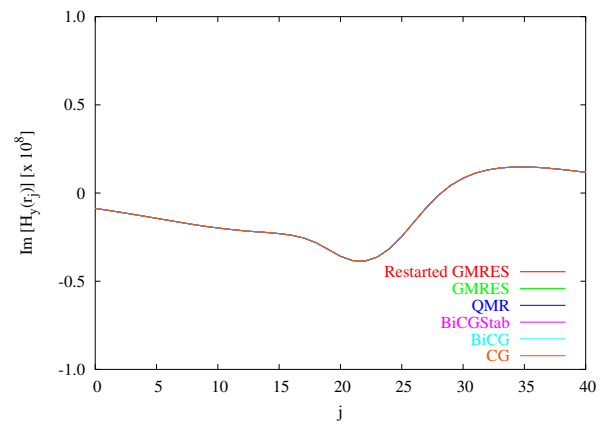
(d)
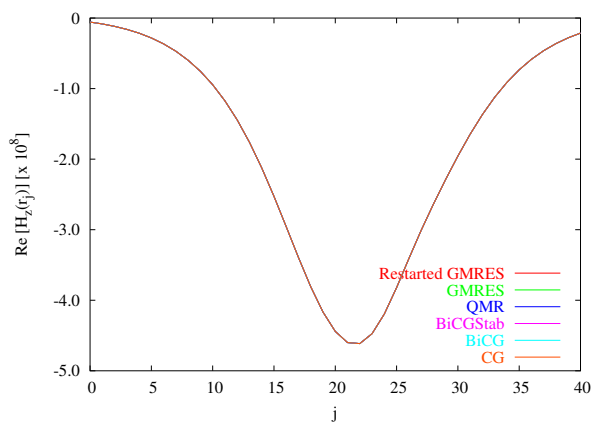
(e)
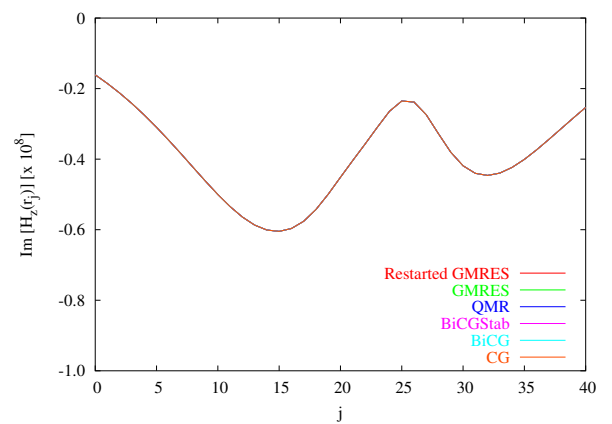
(f)

Fig. 1 - G. Franceschini *et al.*, "A comparative assessment ..."
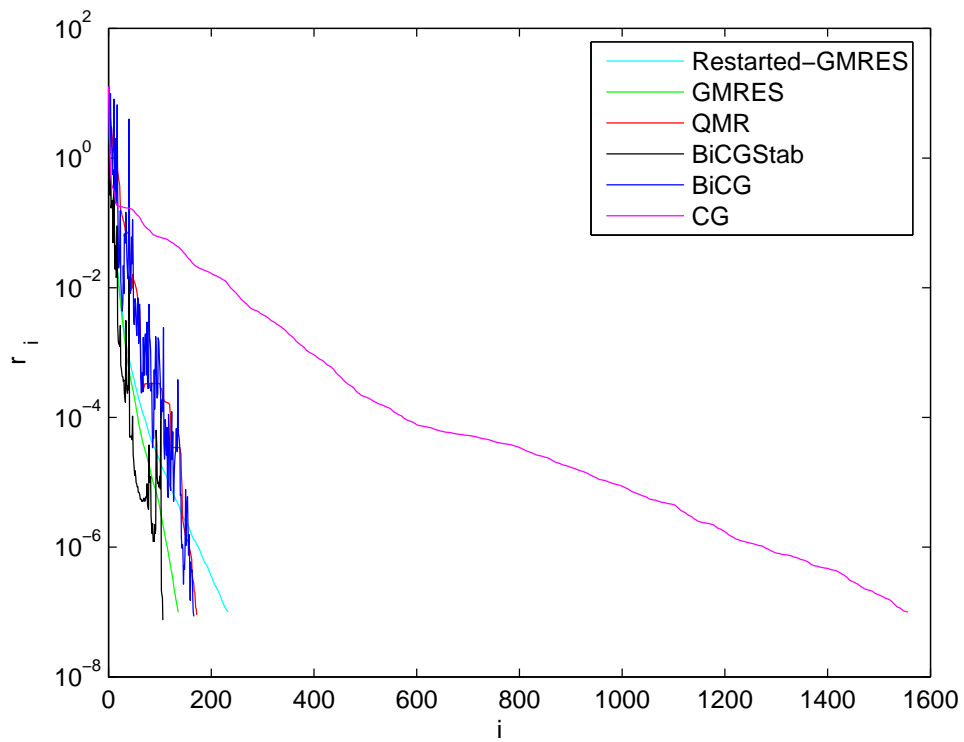
Fig. 2 - G. Franceschini *et al.*, "A comparative assessment ..."
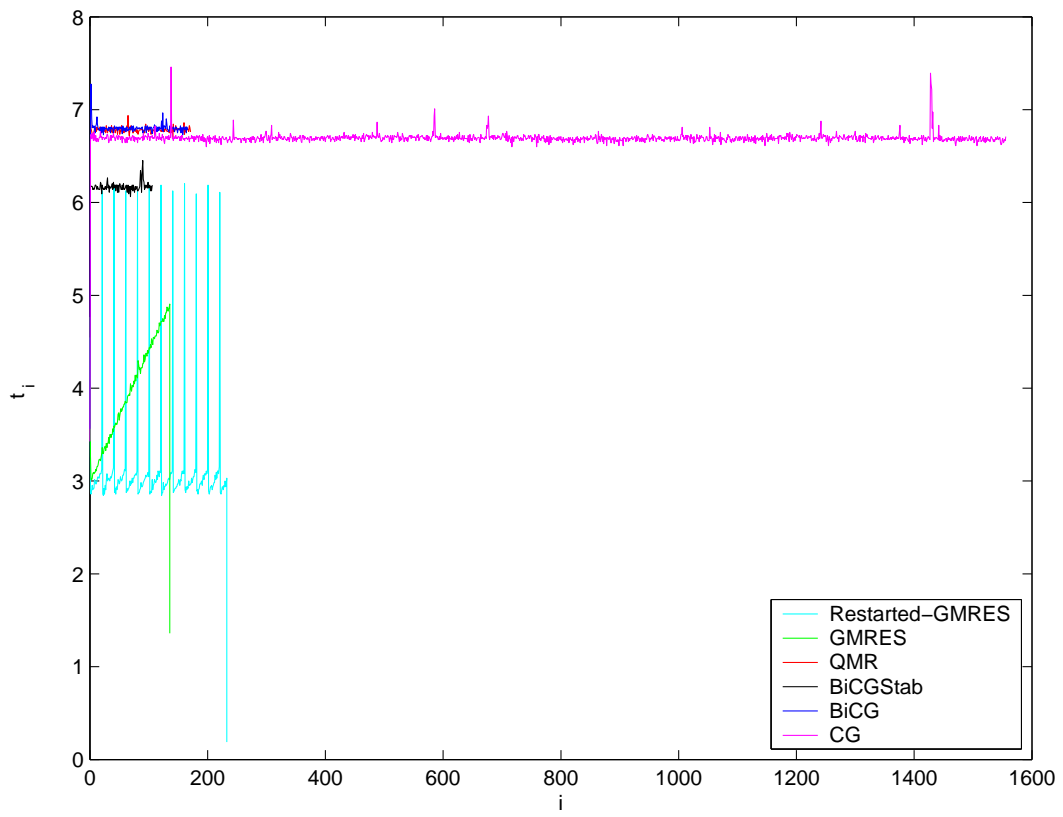
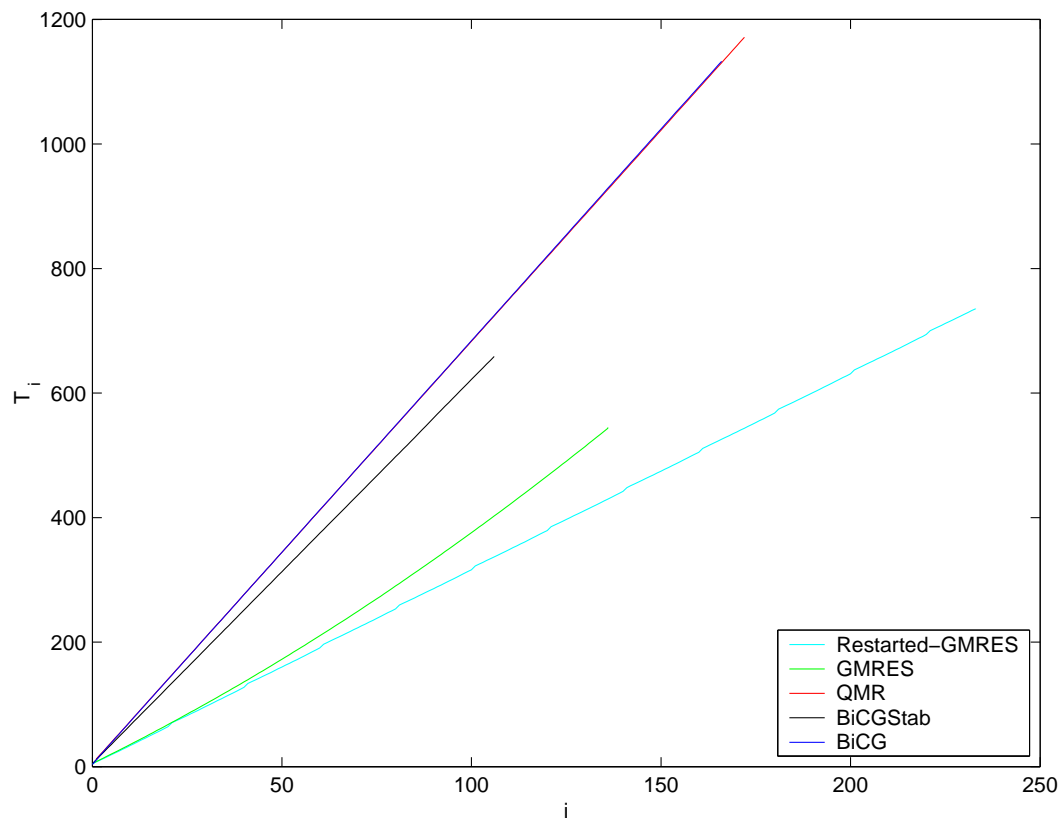Fig. 3 - G. Franceschini *et al.*, "A comparative assessment ..."

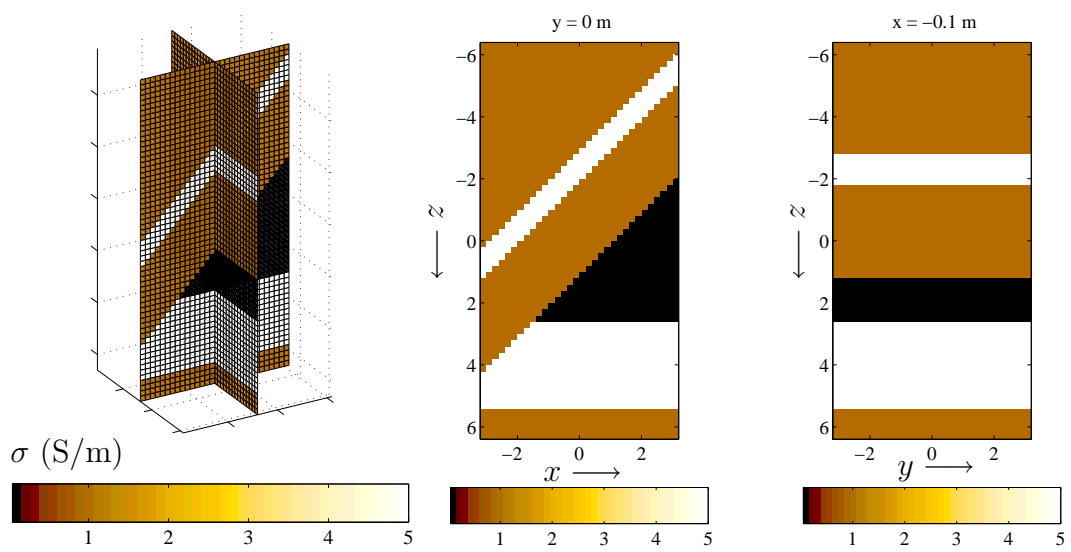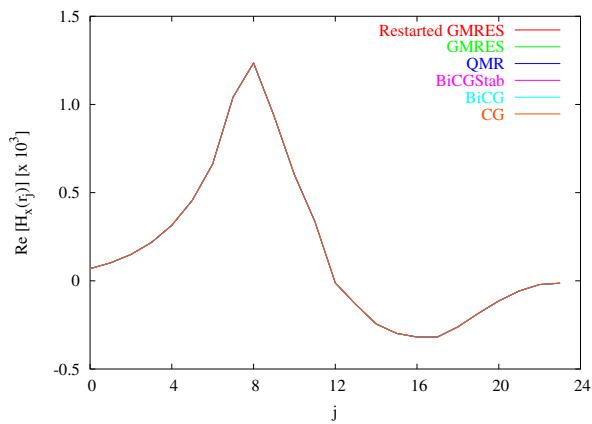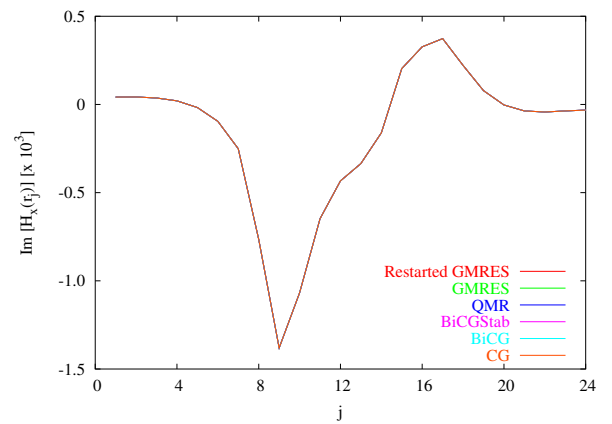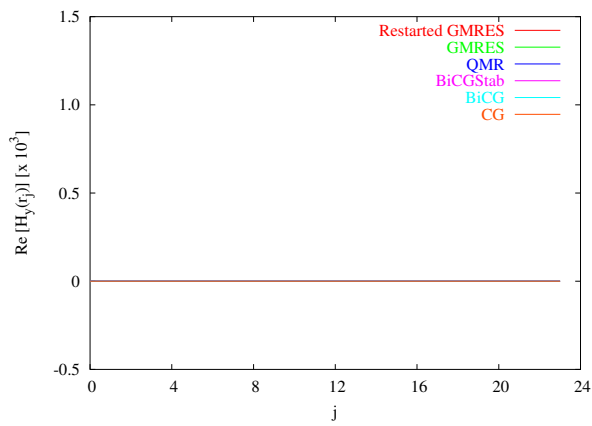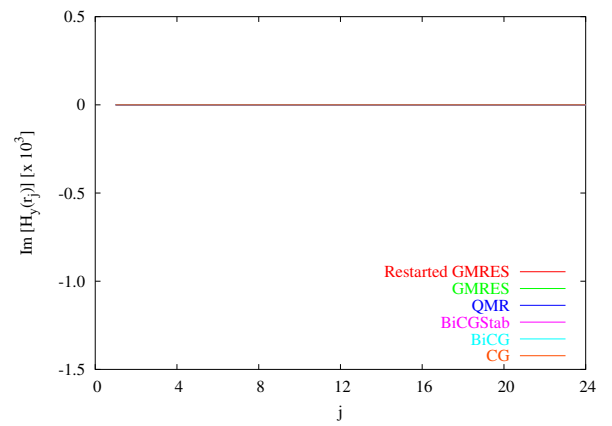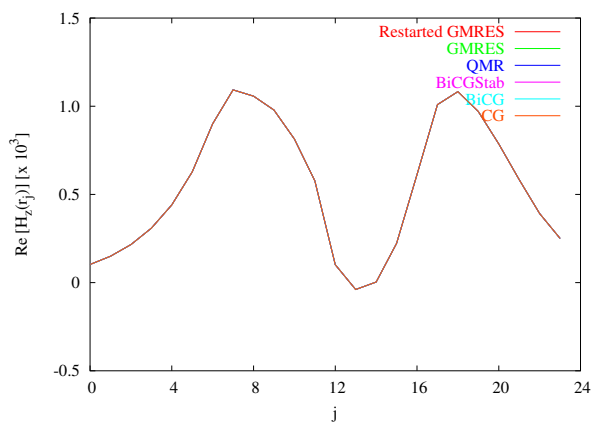**Fig. 4 - G. Franceschini *et al.*,** "A comparative assessment ..."

σ (S/m)

y = 0 m

x = −0.1 m

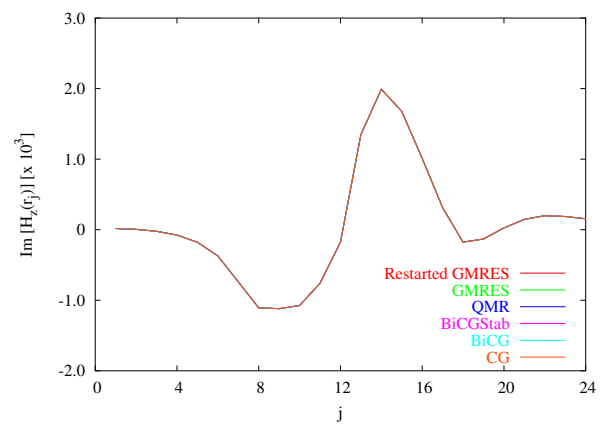Fig. 5 - G. Franceschini *et al.*, "A comparative assessment ..."
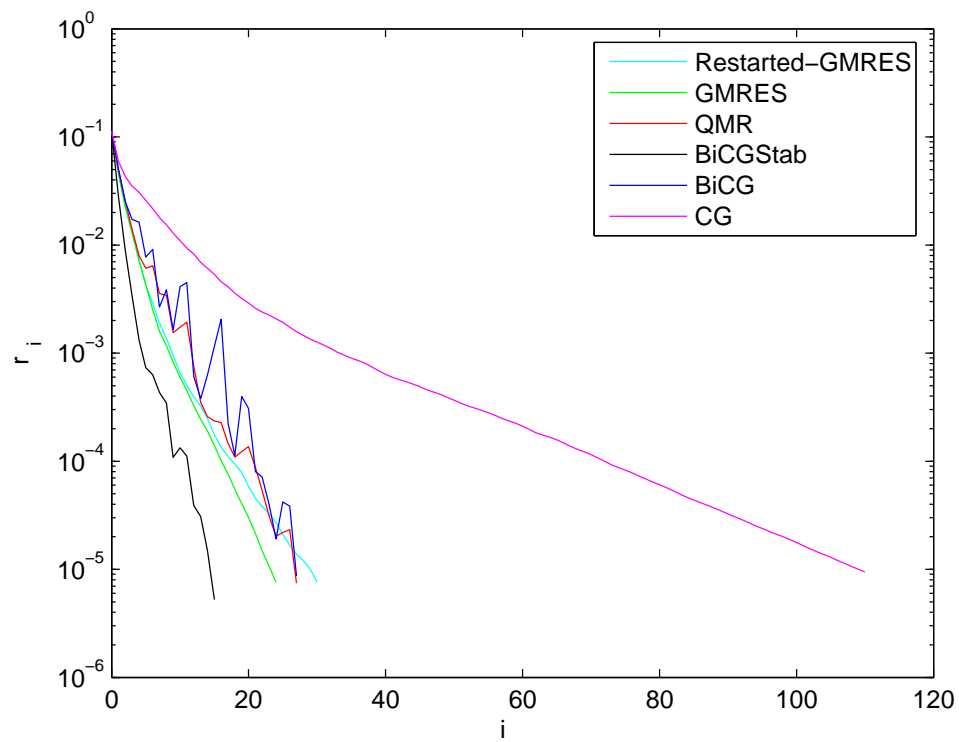
(a)

(b)

(c)

(d)

(e)

(f)

Fig. 6 - G. Franceschini *et al.*, "A comparative assessment ..."

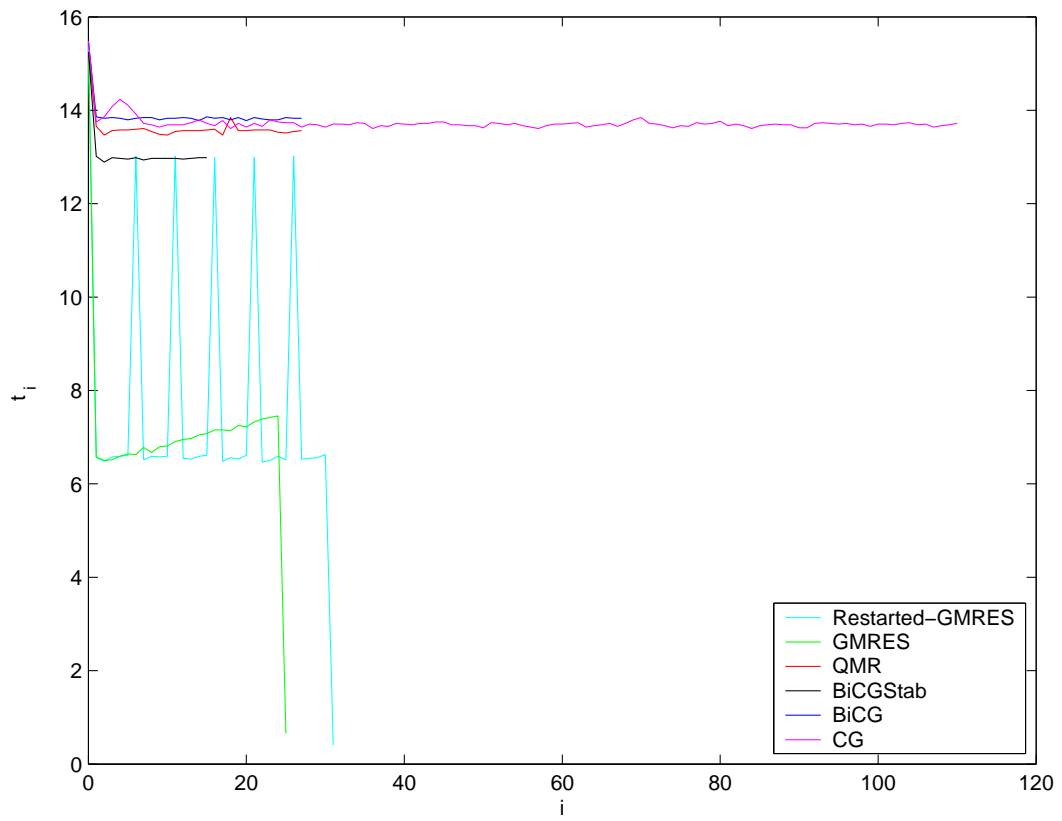Fig. 7 - G. Franceschini *et al.*, "A comparative assessment ..."

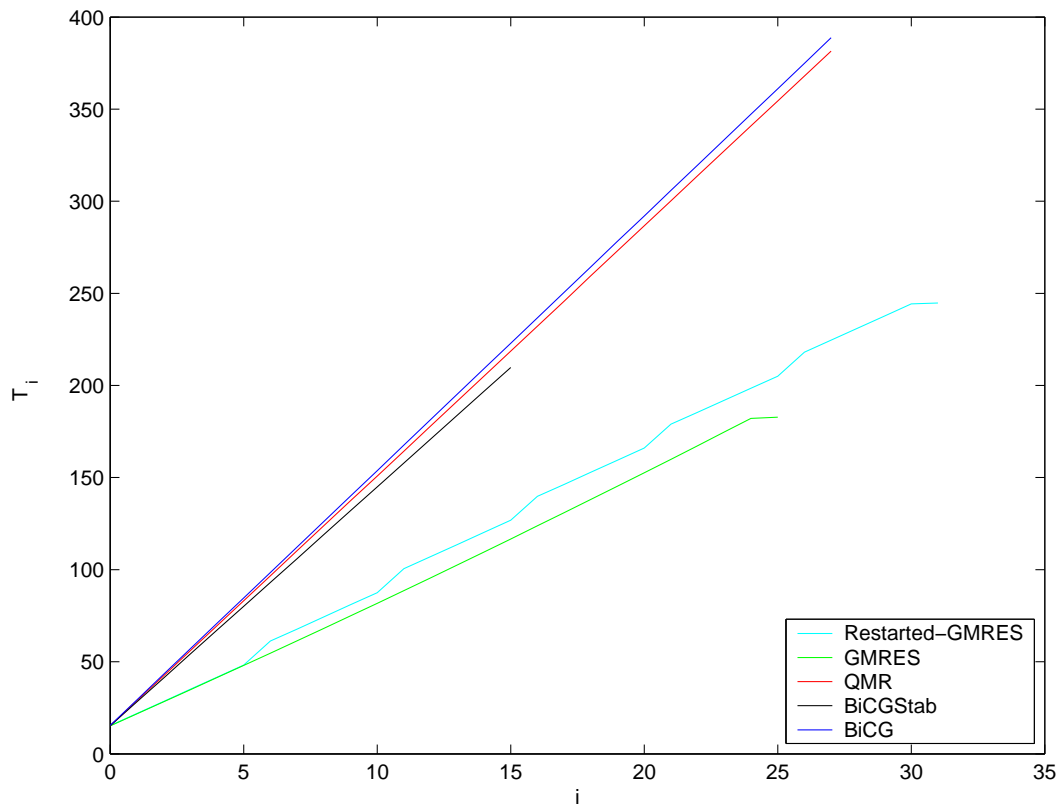Fig. 8 - **G. Franceschini** *et al.*, "A comparative assessment ..."

Fig. 9 - G. Franceschini *et al.*, "A comparative assessment ..."

$Method$	I_{conv}	$t_0 \; [sec]$	$\overline{t_i} \; [sec]$	$T \; [sec]$
$R - GMRES$	233	4.5	3.1	736
$GMRES$	136	4.8	4.0	545
QMR	172	6.9	6.7	1171
$BiCGStab$	106	4.8	6.2	659
$BiCG$	166	5.2	6.8	1133
CG	1556	4.9	6.7	10420

Tab. I - G. Franceschini *et al.*, "A comparative assessment ..."

Method	I_{conv}	t_0 [sec]	$\overline{t_i}$ [sec]	T [sec]
$R - GMRES$	31	15.4	7.4	245
$GMRES$	25	15.2	6.7	183
QMR	27	15.3	13.6	382
$BiCGStab$	15	15.3	13.0	210
$BiCG$	27	15.5	13.9	389
CG	110	15.5	13.7	1524

Tab. II - G. Franceschini *et al.,*"A comparative assessment ..."